GEOPHYSICAL RESEARCH LETTERS, VOL. 22, NO. 8, PAGES 997-1000, APRIL 15, 1995

Broadband analysis of the 21 September, 1993 Klamath Falls earthquake sequence

Douglas Dreger[1], Jeroen Ritsema[2], and Michael Pasyanos[1]

Abstract. The source characteristics of the Klamath Falls earthquake sequence were estimated from broadband seismograms recorded by the Berkeley Digital Seismic Network (BDSN), TERRAscope, and western United States IRIS stations. Solutions were obtained for events ranging in size from M_w3.8 to M_w6.0. An empirical Green's function inverse approach was used to estimate kinematic source parameters of the two M_w6.0 mainshocks. Both events were found to have ruptured northwest on adjacent segments of the Lake of the Woods system of normal faults. The two mainshocks abut where there is a pronounced 10° to 20° clockwise rotation of strike which may have initially acted as a barrier to a through-going M_w6.2 event.

Introduction

An unusual sequence of the largest earthquakes on record to strike Oregon occurred on September 21, 1993. The sequence was located 16 km northwest of the city of Klamath Falls in southern Oregon (Figure 1), and began at 03:16 (UTC; 8:16 pm PDT) with a M_w4.1 foreshock followed by two M_w6.0 mainshocks at 03:29 and 05:45 (UTC), herein referred to as events 0329 and 0545 respectively. The mainshocks were felt to a range of 100 to 150 km, and caused extensive damage in the epicentral area [*Wiley et al.* 1993]. These damaging mainshocks were followed by 10 M_w>4 aftershocks, the largest of which (M_w5.4) occurred on December 4, 1993. There were reports of extensive ground failure and cracking, although none was attributable to tectonic slip on a mapped fault [*Wiley et al.* 1993].

There are Quaternary normal faults throughout the north-northwest trending Klamath basin, the western margin of which is defined by the Lake of the Woods fault zone (LWFZ). The LWFZ is composed of imbricated east dipping normal-slip faults, approximately 8-12 km west of the sequence. Tectonically, the Klamath Basin is within the northwestern Basin and Range province. The Cascade volcanic arc lies to the west, and there are numerous volcanic vents in the epicentral region [*e.g. Luedke et al.* 1983]. Despite the recent volcanic activity and the presence of Quaternary faulting, there have been only a few moderate earthquakes as large as M4.0 historically [*e.g. Wiley et al. 1993; Jacobson, 1986*], making this sequence a unique opportunity to study the source characteristics of earthquakes occurring on normal faults in the region. This paper serves to report on our moment tensor results for the 20 largest events and develops a kinematic source model of the mainshock rupture process.

Moment Tensor Analysis

Three regional distance moment tensor methods using data from BDSN, TERRAscope and western U.S. IRIS stations were applied to the three largest events. Harvard CMT solutions are available for comparison for the two mainshocks. Table 1 lists the methods, data used, references, and solutions. The agreement between the various methods for the three largest events is reasonably good. The largest standard deviation of the mean solutions are 12°, 9° and 20° for the strike, dip and rake parameters respectively. These values are representative of the scatter of the various regional methods in use in California [*Ritsema et al.*, 1994] and more closely reflect the true uncertainties than the standard errors of the individual methodologies because the effects of different data sets, methodologies, and velocity structures are considered. For comparison the standard errors computed for event 2 using method 1 are 2° for all three fault parameters. Scalar seismic moment for

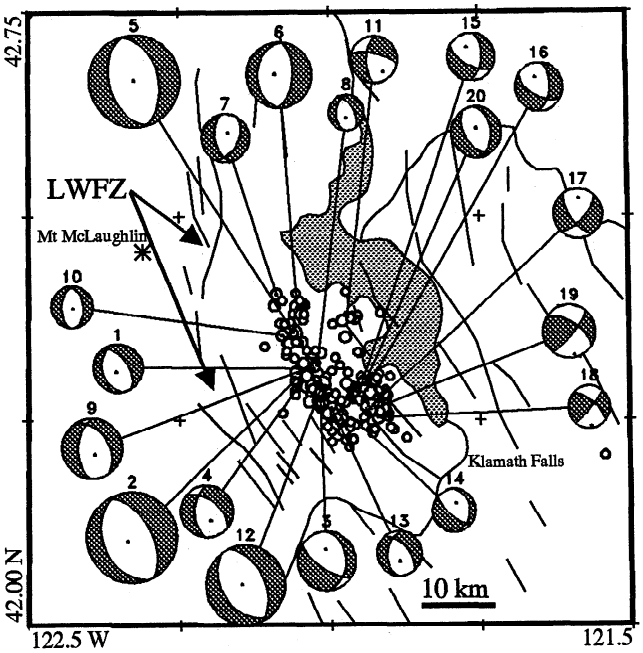

Figure 1. Moment tensor solutions obtained using method 1 (Table 1) and master event relocated aftershocks (Tony Qamar, written communication, 1994) are plotted with Quaternary faults.

[1]Seismographic Station, University of California, Berkeley
[2]Institute of Tectonics, University of California, Santa Cruz

Paper number 95GL00566
0094-8534/95/95GL-00566$03.00

Table 1. Fault Plane Solutions

Ev. #	OT	Lat. (°N)	Lon. (°W)	M_w	M_o (Nm)(km)	Z	S/D/R (°)	M	S #
1	9309210316	42.31	122.02	4.1	1.8 15	8	326/57/-103	1	1
2	9309210329	42.32	122.03	5.9	7.6 17	8	332/55/-94	1	2
				5.9	8.4 17	12	353/37/-59	2	12
				6.0	1.1 18	8	343/46/-83	3	3
				6.0	1.1 18	15	334/60/-98	4	44
3	9309210416	42.27	122.01	4.5	7.2 15	8	358/34/-41	1	1
4	9309210434	42.30	122.04	4.3	2.8 15	5	308/53/-129	1	1
5	9309210545	42.36	122.06	5.9	7.9 17	8	346/46/-89	1	2
				6.0	1.4 18	12	9/37/-46	2	12
				6.0	1.1 18	8	352/47/-84	3	3
				6.0	1.0 18	15	357/34/-85	4	42
6	9309210614	42.39	122.05	4.8	2.0 16	8	3/56/-90	1	1
7	9309210728	42.40	122.09	4.1	1.4 15	8	28/44/-60	1	1
8	9309211734	42.31	122.02	3.5	2.3 14	8	330/56/-113	1	1
9	9309230621	42.31	122.05	4.6	8.7 15	8	328/45/-117	1	1
10	9309240157	42.35	122.08	3.8	5.2 14	8	351/44/-100	1	1
11	9309241653	42.38	121.97	4.0	1.3 15	5	182/63/-22	1	1
12	9312042215	42.29	122.01	5.4	1.4 17	8	335/50/-83	1	2
				5.4	1.5 17	10	330/42/-72	2	9
				5.4	1.6 17	6	326/45/-79	3	3
13	9312042223	42.26	121.99	3.9	8.9 14	5	317/58/-122	1	1
14	9312042250	42.25	121.96	3.9	7.2 14	5	358/27/-46	1	1
15	9312251233	42.28	121.95	4.1	1.5 15	5	3/53/-40	1	1
16	9312311808	42.29	121.94	4.1	1.7 15	5	10/53/-38	1	1
17	9401070939	42.26	121.93	4.1	1.8 15	5	144/63/-155	1	1
18	9401080255	42.25	121.92	3.8	6.0 14	14	308/65/174	1	1
19	9401091903	42.26	121.92	4.3	3.1 15	14	302/60/166	1	1
20	9401192227	42.29	121.94	4.2	2.1 15	5	353/42/-70	1	1

Event locations from UW Geophysics. Ev.: event number. OT: origin time. S/D/R: Strike, dip, rake. M_o: Seismic moment. Z: Centroid depth. M: Methodology where 1 is three-component waveform (f<0.1 Hz); 2 is regional surface wave spectral inversion (f<0.066 Hz; Patton and Zandt, 1991; Romanowicz et al., 1993); 3 is the RCMT method (f< 0.05 Hz; Ritsema and Lay, 1993); 4 is the Harvard CMT (f<0.022 Hz). S: number of stations used in each inversion.

the three largest events vary by as much as 48% which is quite good considering that variations of a factor of two are sometimes observed [*e.g. Ritsema et al.*, 1994]. The three regional methodologies agree very well for event 12 indicating that the greater scatter in the solutions of the two main events may be due to source complexity.

The three regional methodologies obtained minima in the depth parameter space for each of the events analyzed. Table 1 shows that there is a range of 2 to 4 km in the depth estimates of the regional methodologies. Master event relocation of the three largest events (Anthony Qamar, personal communication, 1993) indicate depths of 10.3 km for the two mainshocks and a depth of 6.5 km for event 12 (Table 1) which are in general agreement with the moment tensor results. The depth of the events and the surface projection of the east-dipping plane are consistent with the LWFZ as the causative fault structure. The largest west dipping structure forms the eastern edge of Klamath Lake and is 22 km east-northeast of the epicentral area. Unfortunately, the relocated aftershocks do not define planar structures attributable to specific surface faults.

Figure 1 shows the best fitting double-couple solutions obtained from method 1 (Table 1). The predominantly normal-slip sequence was observed to rotate from northwest striking in the southern half to more northerly striking in the northern half, in agreement with *Braunmiller et al.* [1995]. The standard error of method 1 indicates that the relative mechanism changes are significant although there may be larger systematic errors associated with model assumptions. The solutions for the two mainshocks indicate strike uncertainty of approximately 12°, however each method shows a consistent clockwise rotation of the strike of event 0545 by $9 - 20°$ which agrees with the rotation of Quaternary faulting, and the aftershock distribution (Figure 1). The foreshock and event 0329 are located near the vertex of this structural "knee." The eastern edge of the sequence shows considerably greater variability in focal mechanism estimates including some strike slip events. These events were part of an increase in activity following the December 4, 1993 aftershock (event 13) on a sub-parallel structure approximately 6 km to the east (Figure 1). Although there is some variation in focal mechanisms the T-axes are very stable and strike east-northeast for all of the events studied.

Source Time Functions

We estimated the source durations of the two mainshocks using broadband data recorded at several of the closest BDSN stations and the IRIS station COR using the empirical Green's function deconvolution technique. This method assumes that a small event, or empirical Green's function (EGF), can be viewed as a point-source, and that the deconvolution of the EGF from the mainshock records removes waveform distortions due to propagation leaving the far-field source time function (STF). The data were bandpass filtered between 0.01 to 2 Hz and integrated to displacement prior to the deconvolution. To stabilize the deconvolution process a "water level" of 1% of the peak EGF spectra was used to fill spectral holes.

Event 9 was used as the EGF for 0329 and event 6 was used for 0545. These choices were based on the relative locations, and focal mechanisms, as well as the need to select events for which there is reasonably good signal-to-noise ratios at regional distances. We found that STFs obtained from both the tangential and vertical components, as well as with other aftershocks had similar features. Notably, there is a pronounced thinning of the STF for both mainshocks from the southeast clockwise to the northwest (Figure 2a and 3a). In addition, event 0329 shows two distinct pulses at stations COR, ARC, YBH and WDC indicating a greater degree of source complexity.

The thinning of the STFs toward the northwest suggests directivity in that direction, however STF amplitudes are greatest at stations to the south opposing this hypothesis. The small differences in mainshock-EGF radiation patterns lead to a systematic elevation of STF amplitude at southwest stations and a decrease in amplitude at COR due to the near-nodal position of COR on the focal sphere. Sensitivity tests using synthetic seismograms reveal that while STF amplitudes may be modulated by small differences in the mechanisms the duration and shape were found to be stable.

Source Time Function Inversion

To quantify the directivity and dimension of the two mainshocks a procedure based on the method of *Mori and Hartzell* [1990], and modified for regional distances [*Dreger*, 1994] was used. Essentially this method makes the assumption that STF shape can be mapped into the

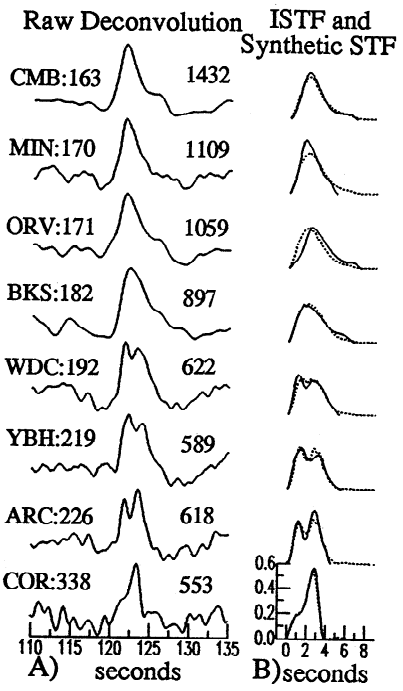

Figure 2. (a) Far-field source time functions obtained by deconvolving the vertical component motions from event 9 from event 0329. The name and azimuth to each station is noted on the left. On the right the peak amplitudes of the raw STFs are plotted. (b) Compares the fit of synthetic STFs (dashed) and the inferred STFs (solid) computed from the best fitting slip model (Figure 4).

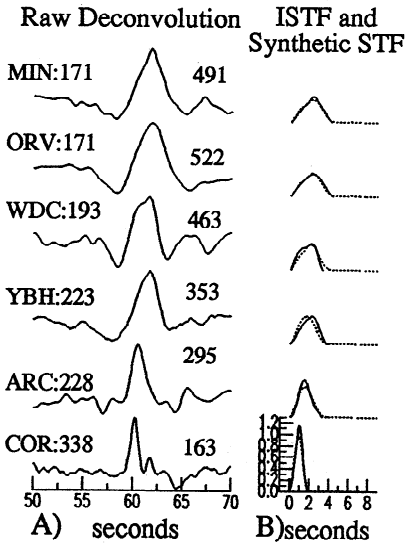

Figure 3. (a) Far-field source time functions obtained by deconvolving the vertical component motions from event 6 from event 0545. The name and azimuth to each station is noted on the left. (b) Compares the fit of synthetic STFs (dashed) and the inferred STFs (solid) computed from the best fitting slip model (Figure 4).

spatial and temporal distribution of fault slip, and constitutes a perturbation to the point-source approximation implied by the deconvolution process. The rupture model consists of a radial rupture front propagating at constant velocity with slip distributed across a plane with the orientation of the mainshock. The plane is discretized into subfaults which are allowed to slip only once following the passage of the rupture front. Since it would be difficult to confidently isolate individual wave types we assume a half space ray trajectory to compute relative subfault-hypocenter distances, and timing using an assumed shear wave velocity of 3.6 km/s. Absolute slip is computed using independent long-period scalar seismic moment estimates and is subject to the same uncertainty. For the Klamath Falls earthquakes the slip amplitudes have an uncertainty of approximately 48%.

To be consistent at all of the stations, the STF used in the inversion were interpreted between zero crossings. In addition, to give each station equal weight in the inversion and to remove amplitude uncertainty, the STF were normalized to unit area. Thus the method fits STF shape only. The computed areas for events 0329 and 0545 were found to have standard deviations of 41% and 55% of their respective mean values.

In our calculations a 21 x 23 km fault (strike by downdip width) was used and the plane was discretized into 483 1 km x 1 km subfaults. Subfault STF are approximated by "boxcar" functions. Assuming a duration (T_d) of 1 s the spatial resolution (λ) of the model is approximately 2.2 km or twice the grid spacing ($\lambda = V_r T_d$). An inversion in which the subfault dimension was increased to 4 km^2 resulted in the same gross slip distribution. Inversions were performed over a range of rupture velocity (1.8 to 3.4 km/s) to find the best combination of model parameters.

The fit to the data is shown in Figures 2b and 3b. Figure 4 shows the distribution of slip on the east dipping fault plane. The M_0 estimated from method 1 (Table

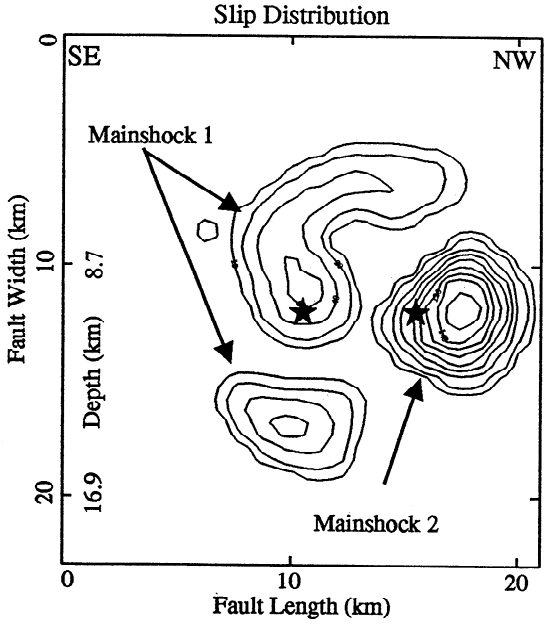

Figure 4. Slip distribution. The star denotes the hypocentral locations of both main-events. The slip attributable to each mainshock is labeled. These results were obtained with a rupture velocity of 2.2 km/s (60 % of the assumed shear wave velocity of 3.6 km/s). The first and second contours are the 10 and 20 cm level. Subsequent contours show increments of 20 cm in slip.

1) was used to scale the absolute slip. A shallow minimum in variance was obtained for a rupture velocity of 2.2 km/s. Event 0329 had components of both up- and downdip rupture. The updip slip patch extends to the northwest. Event 0545 ruptured a relatively smaller region located west of its hypocenter with higher average stress drop. Event 0329 abuts against the slip patch of event 0545 and the region where the surface faults and focal mechanisms undergo a rotation in strike. It is possible that the warped fault may have initially impeded the rupture from propagating into the event 0545 slip area.

Discussion

In *Dreger* [1994] the sensitivity of the method was discussed. In brief, those tests revealed that the deconvolution procedure is sensitive to the relative depths of the main events and their EGFs. The optimal location is near the slip centroid. Deconvolutions using sub-optimally located EGFs resulted in noisy STFs which would be nearly impossible to interpret. These tests also investigated the assumption of direct subfault-station ray paths in a dispersive medium. Since in the test case and also for the Klamath Falls earthquakes the fault dimension is approximately 10% of the propagation distance, these influences were found to be small but capable of introducing noise into the slip maps. Hypocenter uncertainty impacts the absolute location of slip but it does not affect the hypocenter-relative position. Nevertheless it was found that the approach can effectively recover the main slip patches.

Unfortunately there is no west-northwest or east-northeast station coverage and it was not possible to constrain which of the two planes slipped from the STF data alone. As discussed previously, the east dipping plane is favored because of the geometrical relationship with a surface mapped fault. The 0329 data seems to prefer a component of downdip slip to fit the STF complexity at ARC, COR, YBH and WDC, however the resolution is poor. If we limit the allowable dimension of the fault such that there is only updip rupture, a patch of low amplitude slip develops south of the hypocenter to compensate and the fit to the data is reasonably good. Alternatively, the subevent could be caused by temporal rather than spatial complexity, or possibly by rupture on a subparallel fault, either of which are not resolvable with the approach and assumptions we employed. It is therefore safest to interpret only the robust updip slip patch of event 0329 and the northward directivity of both events.

Conclusion

Geometrically the east dipping LWFZ is the most likely causative fault structure. There is a pronounced structural "knee" in the surface expression of the LWFZ that is also evident in the moment tensor solutions and the aftershock distribution indicating that the complexity persists to seismogenic depths. The directivity analysis revealed that both events had a component of northwest rupture. These events occurred on abutting segments of the LWFZ. We propose that the pronounced change in strike of the causative fault structure acted as a barrier to a through-going M_w 6.2 event. This observation agrees with those made by *King and Nábělek* [1985] for other moderate to large earthquakes in which ruptures were found to either initiate or terminate near fault bends.

Acknowledgments. We thank the University of Washington Geophysics for making their first-motion results and the Klamath Falls fault map available. This study was partially supported by USGS award numbers 1434-94-G2311 (DD) and 1434-94-G2442 (JR), and is contribution no. 94-9 of the Berkeley Seismographic Station and no. 256 of the Institute of Tectonics.

References

Braunmiller, J., J. Nábělek, and B. Leitner, The 1993 Klamath Falls, Oregon earthquake sequence: Source mechanisms from regional data, *In press Geophys. Res. Lett.*, 1995.

Dreger, D. S., Empirical Green's Function Study of the January 17, 1994 Northridge, California Earthquake, *Geophys. Res. Lett., 21,* 2633-2636, 1994.

Jacobson, R. S., Map of Oregon Seismicity, 1841-1986, *Oregon Department of Geology and Mineral Industries Geological Map Series, GMS-49,* 1986.

King, G. C. P., and J. L. Nábělek, The Role of Bends in Faults in the Initiation and Termination of Earthquake Rupture, *Science, 228,* 984-987, 1985.

Luedke, R. G., R. L. Smith, and S. L. Russel-Robinson, Map Showing Distribution, Composition and Age of Late Cenozoic Volcanoes and Volcanic Rocks of the Cascade Range and Vicinity, Northwestern United States, *U.S.G.S. Miscellaneous Investigations Series, Map I-1507,* 1983.

Mori, J., and S. Hartzell, Source Inversion of the 1988 Upland Earthquake:Determination of a Fault Plane for a Small Event, *Bull. Seism. Soc. Am., 80,* 507-518, 1990.

Patton, H. J., G. Zandt, Seismic Moment Tensors of Western U.S. Earthquakes and Implications for the Tectonic Stress Field, *J. Geophys. Res., 96,* 18245-18259, 1991.

Ritsema, J., and T. Lay, Rapid Source Mechanism Determination of Large (M_w >=5) Earthquakes in the Western United States, *Geophys. Res. Lett., 20,* 1611-1614, 1993.

Ritsema, J. T. Lay, D. Dreger, M. Pasyanos, and B. Romanowicz, Moment Tensor Inversion for Western United States Earthquakes: Calibration of Methods, *Seism. Res. Lett., 65,* p 33, 1994.

Romanowicz, B. D. Dreger, M . Pasyanos, and R. Urhammer (1993). Monitoring of Strain Release in Central and Northern California Using Broadband Data, *Geophys. Res. Let.,* 20, 1643-1646.

Wiley, T. J., D. R. Sherrod, D. K. Keefer, A. Qamar, R. L. Schuster, J. W. Dewey, M. A. Mabey, G. L. Black, and R. E. Wells, Klamath Falls Earthquakes, September 20, 1993 - Including the Strongest Quake Ever Measured in Oregon, *Oregon Geol., 55,* 127-134, 1993.

D. Dreger & M. Pasyanos, Seismographic Station, University of California, Berkeley, CA 94720.

J. Ritsema, Institute of Tectonics, University of California, Santa Cruz, CA 95064.

(received April 25, 1994; revised August 29, 1994; accepted October 18, 1994.)